Zeolite Synthesis

DOI: 10.1002/ange.201302672

Solvent-Free Synthesis of Silicoaluminophosphate Zeolites**

Yinying Jin, Qi Sun, Guodong Qi, Chengguang Yang, Jun Xu, Fang Chen, Xiangju Meng, Feng Deng,* and Feng-Shou Xiao**

Microporous crystalline aluminosilicate and silicoaluminophosphate zeolites are currently regarded as the most useful zeolite catalysts for industrial processes.[1] For example, aluminosilicate Y zeolite is efficient for fluid catalytic cracking,[2] and silicoaluminophosphate SAPO-34 zeolite is a selective catalyst for the formation of light olefins from methanol.[3] Notably, the synthesis of these zeolites usually requires the presence of solvents such as water and alcohols under hydrothermal, solvothermal, or ionothermal conditions.[1–12] The use of solvents normally results in polluted water, reduced synthesis efficiency owing to autoclave space being used by the solvent, and generates high pressure under high-temperature solvothermal conditions.[4] The ionothermal route, which has been successfully developed for synthesizing aluminophosphate-based zeolites, can effectively eliminate the high pressure problem, because of the low vapor pressure of ionic liquids.[5,6] Recently, Ren et al. reported the solvent-free synthesis of aluminosilicate zeolites with the advantage of reducing waste production and increasing zeolite yield, as well as eliminating high pressure.[4b] Morris et al. have also highlighted the importance of solventless synthesis,[7] but this route has still not been successfully applied to the synthesis of aluminophosphate-based zeolites.

Herein, we report the solvent-free synthesis of silicoaluminophosphate (SAPO-34, SAPO-11, SAPO-20, and SAPO-43), aluminophosphate (APO-11), and heteroatom-containing aluminophosphate (M-APO-11 and M-SAPO-46; M = Co or Mg) zeolites by mixing, grinding, and heating the raw materials. The solvent-free synthesis of SAPO-34 (S-SAPO-34) is carefully investigated as a model reaction. Importantly, S-SAPO-34 exhibits good catalytic performance in catalytic tests for methanol-to-olefin (MTO) conversion.

Figure 1 shows X-ray diffraction (XRD) pattern, N_2 sorption isotherms, scanning electron microscopy (SEM), and transmission electron microscopy (TEM) images of calcined S-SAPO-34. XRD patterns show well-resolved peaks in the range of 4–40° (Figure 1 A), which are in good agreement with that of a CHA zeolite structure.[8] N_2 sorption isotherms of the sample (Figure 1 B) exhibit a steep increase in the curve at a relative pressure of $10^{-6} < P/P_0 < 0.01$, which is due to the filling of micropores.[4a] Additionally, at a relative pressure of 0.50–0.98, a hysteresis loop can be observed, which suggests that the sample is both meso- and macroporous.[9] Accordingly, the sample Barrett—Joyner—Halenda (BJH) pore-size distribution appears at 11 nm and ca. 100 nm (Figure 1 C). The Brunauer—Emmett—Teller (BET) surface area and pore volume are 459 $m^2 g^{-1}$ and 0.27 $cm^3 g^{-1}$, respectively.

Figure 1 D and E show low and high magnification SEM images of the sample. The low magnification image (Figure 1 D) shows that the sample has very uniform cubic morphology, with particle sizes of 10–30 μm. The high magnification image (Figure 1 E) clearly shows hierarchical macropores of 0.1–3 μm.

The sample TEM images (Figure 1 F) show the presence of hierarchical mesopores (5–50 nm). The chemical composition of the sample was determined by ICP, as shown in the Supporting Information, Table S1. Based on the above results, it can be concluded that the S-SAPO-34 sample has a unique structure consisting of micro-, meso-, and macropores. This kind of structure has been considered as an important development for designing and preparing efficient catalysts.[10]

Figure 2 shows ^{27}Al, ^{31}P, and ^{29}Si magic-angle spinning (MAS) NMR spectra of as-synthesized S-SAPO-34 and calcined S-SAPO-34. The ^{27}Al MAS NMR spectrum of S-SAPO-34 (Figure 2 A-a) exhibits two peaks at 41.9 and 10.3 ppm. The peak at 41.9 ppm was assigned to 4-coordinated Al species in the zeolite framework,[13] and the peak at 10.3 ppm may be attributable to 5-coordinated Al species resulting from the coordination of tetrahedral Al sites to organic templates.[14] After calcination, the peak at 40.4 ppm is dominant, and a new peak from 6-coordinated Al species in calcined S-SAPO-34 appears at −8.5 ppm, which is associated with the interaction between the 4-coordinated Al species and water molecules (Figure 2 A-b). This phenomenon can be explained by sample calcination eliminating the coordination between the tetrahedral Al species and the organic templates, allowing interaction between the Al species and water to

[*] Y. Jin, Q. Sun, F. Chen, Dr. X. Meng, Prof. F.-S. Xiao
Department of Chemistry, Zhejiang University
Hangzhou 310028 (P.R. China)
E-mail: mengxj@zju.edu.cn
fsxiao@zju.edu.cn
Homepage: http://www.chem.zju.edu.cn/xiaofs/index-en.html
G. Qi, Dr. J. Xu, Prof. F. Deng
State Key Laboratory of Magnetic Resonance and Atomic and Molecular Physics
Wuhan Institute of Physics and Mathematics, Chinese Academy of Sciences
Wuhan 430071 (P.R. China)
C. Yang
State Key Laboratory of Inorganic Synthesis and Preparative Chemistry, Jilin University (P.R. China)

[**] This work was supported by the Natural National Science Foundation of China (U1162201, 21003107, and 21203165), National High-Tech Research and Development program of China (2013AA065301), and Fundamental Research Funds for the Central Universities (2013XZZX001).

Supporting information for this article is available on the WWW under http://dx.doi.org/10.1002/anie.201302672.

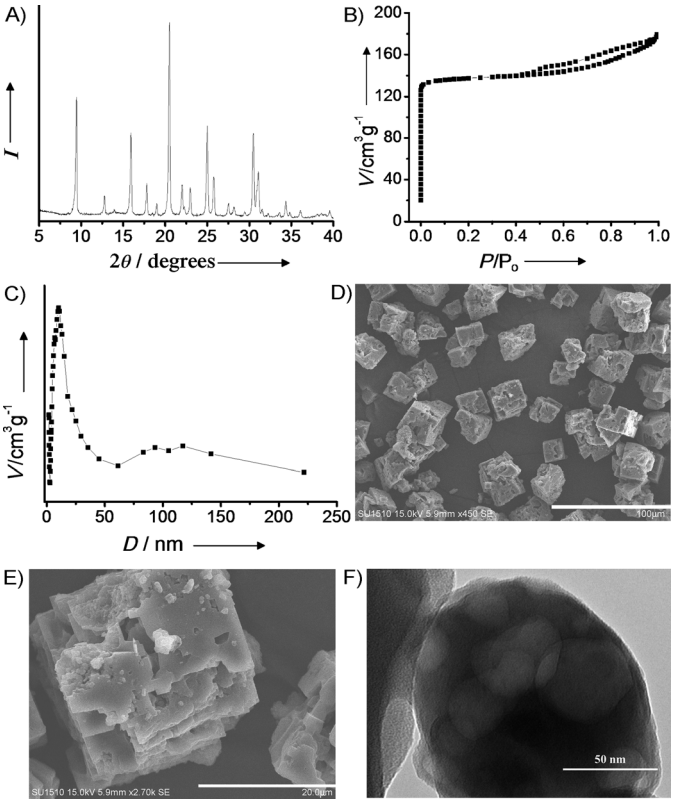

Figure 1. Analytical data for calcined S-SAPO-34. A) XRD pattern, B) N_2 sorption isotherms, C) BJH pore size distribution, D) SEM image (scale bar 100 μm), E) SEM (scale bar 20 μm), and F) TEM image (scale bar 50 nm).

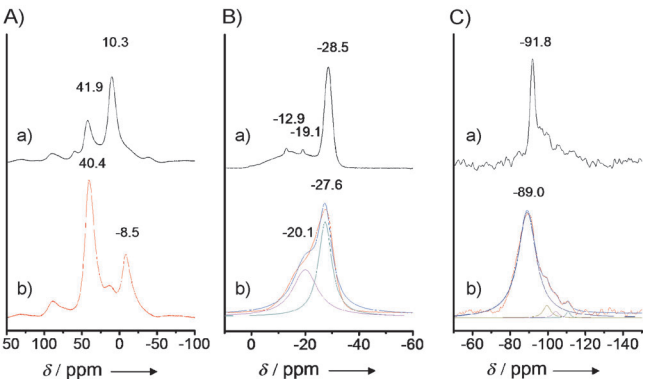

Figure 2. NMR spectroscopic comparison of (a) as-synthesized and (b) calcined S-SAPO-34. A) ^{27}Al, B) ^{31}P, and C) ^{29}Si NMR spectra.

occur. Notably, S-SAPO-34 has a much stronger 10.3 ppm peak intensity than conventional hydrothermally synthesized SAPO-34,[13c] which suggests that the interaction of Al species with organic templates in S-SAPO-34 is much stronger than that in conventional SAPO-34. This strong coordination ability could be favorable for filling organic templates in the zeolite framework.

The ^{31}P NMR spectrum of as-synthesized S-SAPO-34 (Figure 2 B-a) exhibits one strong peak at −28.5 and two weak peaks at −12.9 and −19.1 ppm. The strong peak at −28.5 ppm was assigned to 4-coordinated P species in the zeolite framework,[15] and the two weak peaks at −12.9 and −19.1 ppm may be related to the interaction between the tetrahedral P sites with organic templates and with water, respectively.[16] After calcination, the sample shows a strong peak at −27.6 ppm and a weak peak at −20.1 ppm, whereas the peak at −12.9 ppm completely disappears (Figure 2 B-b), which is in good agreement with the removal of organic templates in the calcined S-SAPO-34. The ^{29}Si MAS NMR spectrum of S-SAPO-34 (Figure 2 C-a) shows a major peak at −91.8 ppm and some weak peaks in the range of −96–−112 ppm, which were assigned to the various Si species (Si(nAl); $n = 4$, 3, 2, 1, and 0).[17] After calcination, these peaks are still present in the sample (Figure 2 C-b), suggesting that both as-synthesized and calcined samples have various Si species, but Si(4Al) species are dominant.

Figure S1 shows the temperature programmed desorption of ammonia curve for calcined S-SAPO-34, which gives two peaks centered at 192 and 417 °C that were attributed to weak and strong acidic sites in the sample. These acidic properties are comparable with those of conventional hydrothermally synthesized SAPO-34.[13a]

Figure 3 shows the catalytic performance of calcined S-SAPO-34 for the methanol-to-olefin (MTO) conversion reaction as a function of reaction time at 400 °C. The catalyst gives full conversion and high selectivities for light olefins including ethylene, propylene, and butylene. The total yield is as high as 88.9 % (150 min), which is comparable with that of conventional hydrothermally synthesized SAPO-34 (91.3 %; Figures S2 and S3). Moreover, the S-SAPO-34 catalyst shows slightly lower selectivity for ethylene, but slightly higher selectivity for propylene and butylene, which is in good agreement with the fact that the hierarchically porous zeolites are favorable for enhancing propylene and butylene selectivities and reducing ethylene selectivity.[12]

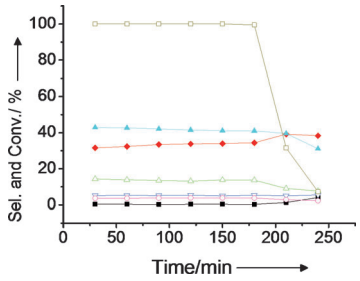

Figure 3. Catalytic conversion (conv.) and product selectivity (sel.) of S-SAPO-34 for MTO conversion at 400 °C. C_3 alkene (▲), C_2 alkene (◆), C_4 alkene (△), C_{4-5} alkanes (○), C_3 alkane (▽), C_2 alkane (■), conversion (□).

Figure 4 shows photographs, XRD patterns, SEM images, and N_2 sorption isotherms of S-SAPO-34 crystallization. The photographs indicate that the crystallization is a solid process (Figure 4 A). Notably, the sample volume is remarkably reduced after the treatment, which is due to the condensation for synthesizing the S-SAPO-34 zeolite. XRD patterns of the

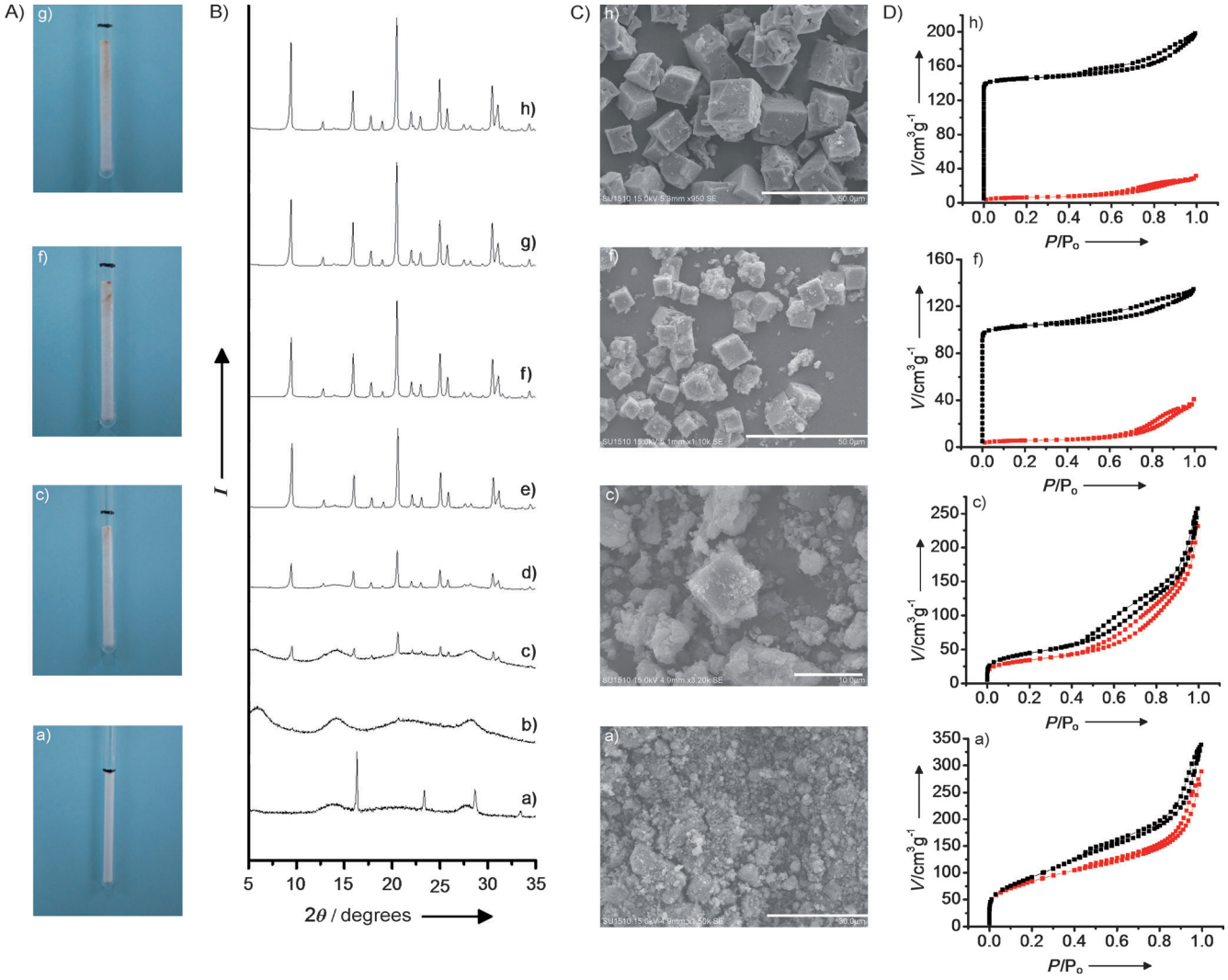

Figure 4. S-SAPO-34 crystallization study. A) Photographs, B) XRD patterns, C) SEM images (scale bars: a) 30 μm, c) 10 μm, f) 50 μm, h) 50 μm), and D) N_2 sorption isotherms (as-synthesized (■), calcined (■)) of the samples crystallized for a) uncrystallized, b) 1 h, c) 2 h, d) 3 h, e) 4 h, f) 8 h, g) 24 h, and h) 36 h for synthesizing the S-SAPO-34 zeolite.

samples (Figures 4B and S4) show that the starting materials have sharp peaks associated with $NH_4H_2PO_4$ (Figure 4B-a). After treatment at 200 °C for 1 h, the sharp peaks completely disappear, becoming amorphous (Figure 4B-b). After heating at 200 °C for 2 h, the sample shows weak peaks associated with the CHA structure, indicating that a small amount of SAPO-34 crystals were been formed (Figure 4B-c). A cubic crystal can be observed in the SEM image (Figure 4C-c). However, N_2 sorption isotherms of the sample show only a small amount of microporosity (21 $m^2 g^{-1}$), thus confirming that a small amount of SAPO-34 crystals were formed. As the crystallization time was increased from 3 h to 8 h, the intensities of XRD peaks gradually increased, indicating the successful solid transformation of S-SAPO-34 from the amorphous phase. As observed in the SEM image (Figure 4C-f) and N_2 sorption isotherms (Figure 4D-f), the cubic crystals are dominant and the micropore surface area is as high as 310 $m^2 g^{-1}$ at 8 h. A further increase in crystallization time from 8 h to 24 h resulted in the disappearance of the amorphous phase (Figure 1D), and N_2 sorption isotherms confirm that the sample is mesoporous (Figure 1B). When the crystallization time is over 24 h, there is no obvious change in the XRD pattern, N_2 sorption isotherms, or SEM image (Figure 4B-h,C-h and D-h), which indicates that the crystallization of S-SAPO-34 is almost finished and that the crystallization of S-SAPO-34 zeolite results from the solid phase transformation.

Calcination of as-synthesized S-SAPO-34 that was crystallized at 8 h and 36 h results in the formation of micropores (Figure 4D-f & D-h), indicating that morpholine acts as a template for micropores in the sample. Meanwhile, mesopores and macropores were also observed in all S-SAPO-34 samples crystallized at various times (Figure 4D). Clearly, the formation of meso- and macrostructures in the crystals might be related to the presence of meso- and macropores in the starting materials and the solid transformation process of zeolite crystals.

Furthermore, we have extended this solvent-free route to synthesize other types of silicoaluminophosphate zeolites, including S-SAPO-11, S-SAPO-20, and S-SAPO-43, all with good crystallinity (Figure S5–S7). Moreover, this solvent-free route was also applied to prepare aluminophosphate- and heteroatom-containing aluminophosphate zeolites, including S-APO-11, S-Co-APO-11, S-Mg-APO-11, S-Co-SAPO-46, and S-Mg-SAPO-46 (Figure S8–S11). The detailed characterization of these samples is still in progress.

In summary, silicoaluminophosphate zeolites with zeolite frameworks of CHA, AEL, SOD, and GIS have been successfully synthesized through a solvent-free route by mechanically mixing the raw materials, followed by heating in the closed vessel. As a typical example, the zeolite product S-SAPO-34 exhibits similar acidic and catalytic properties to that of conventional hydrothermally synthesized SAPO-34 zeolite. Compared with the hydrothermal route, the solvent-free synthesis has obvious advantages: 1) A significant reduction in water pollution. Avoiding the use of solvents in the synthesis greatly reduces the waste generated. 2) Highly efficient use of autoclaves (Table S2). For example, the solvent-free route gives 0.94 g of the S-SAPO-34 product, whereas only 0.51 g of SAPO-34 could be produced by the hydrothermal route in the same autoclave. 3) Low pressure; the lack of solvents greatly decreases the reaction pressure, compared with the hydrothermal route. 4) Hierarchical micro-, meso-, and macrostructures. Taking all of these features into account, it is believable that the solvent-free route for synthesizing aluminophosphate-based zeolites will be of great importance for industrial production in the future. In particular, SAPO-34 and SAPO-11 are efficient catalysts for the industrial processes of MTO conversion and hydroisomerization, respectively.[3,11]

Received: April 1, 2013
Revised: June 4, 2013
Published online: July 10, 2013

Keywords: aluminophosphates · silicoaluminophosphates · solvent-free synthesis · synthetic methods · zeolites

[1] a) A. Corma, *Chem. Rev.* **1995**, *95*, 559 – 614; b) A. Corma, *Chem. Rev.* **1997**, *97*, 2373 – 2419; c) M. E. Davis, *Nature* **2002**, *417*, 813 – 821; d) C. S. Cundy, P. A. Cox, *Chem. Rev.* **2003**, *103*, 663 – 701.

[2] a) U. Navarro, C. A. Trujillo, A. Oviedo, R. Lobo, *J. Catal.* **2002**, *211*, 64 – 74; b) D. Karami, S. Rohani, *Rev. Chem. Eng.* **2007**, *23*, 1 – 34; c) J. García-Martínez, K. Li, G. Krishnaiah, *Chem. Commun.* **2012**, *48*, 11841 – 11843.

[3] a) M. Hartmann, L. Kevan, *Chem. Rev.* **1999**, *99*, 635 – 663; b) W. Song, J. F. Haw, J. B. Nicholas, C. S. Heneghan, *J. Am. Chem. Soc.* **2000**, *122*, 10726 – 10727; c) G. Liu, P. Tian, J. Li, D. Zhang, F. Zhou, Z. Liu, *Microporous Mesoporous Mater.* **2008**, *111*, 143 – 149; d) H. Yang, Z. Liu, H. Gao, Z. Xie, *J. Mater. Chem.* **2010**, *20*, 3227 – 3231; e) J. Li, Y. Wei, J. Chen, P. Tian, X. Su, S. Xu, Y. Qi, Q. Wang, Y. Zhou, Y. He, Z. Liu, *J. Am. Chem. Soc.* **2012**, *134*, 836 – 839; f) H.-G. Jang, H.-K. Min, J. K. Lee, S. B. Hong, G. Seo, *Appl. Catal. A* **2012**, *437*, 120 – 130.

[4] a) R. Xu, W. Pang, J. Yu, Q. Huo, J. Chen, *Chemistry of Zeolites and Related Porous Materials*, Wiley, Singapore, **2007**; b) L. Ren, Q. Wu, C. Yang, L. Zhu, C. Li, P. Zhang, H. Zhang, X. Meng, F.-S. Xiao, *J. Am. Chem. Soc.* **2012**, *134*, 15173 – 15176.

[5] a) E. R. Cooper, C. D. Andrews, P. S. Wheatley, P. B. Webb, P. Wormald, R. E. Morris, *Nature* **2004**, *430*, 1012 – 1016; b) E. R. Parnham, R. E. Morris, *Acc. Chem. Res.* **2007**, *40*, 1005 – 1013; c) R. E. Morris, *Chem. Commun.* **2009**, 2990 – 2998.

[6] a) Y. Xu, Z. Tian, S. Wang, Y. Hu, L. Wang, B. Wang, Y. Ma, L. Hou, J. Yu, L. Lin, *Angew. Chem.* **2006**, *118*, 4069 – 4074; *Angew. Chem. Int. Ed.* **2006**, *45*, 3965 – 3970; b) H. Ma, Z. Tian, R. Xu, B. Wang, Y. Wei, L. Wang, Y. Xu, W. Zhang, L. Lin, *J. Am. Chem. Soc.* **2008**, *130*, 8120 – 8121; c) R. Cai, Y. Liu, S. Gu, Y. Yan, *J. Am. Chem. Soc.* **2010**, *132*, 12776 – 12777.

[7] R. E. Morris, S. L. James, *Angew. Chem.* **2013**, *125*, 2217 – 2219; *Angew. Chem. Int. Ed.* **2013**, *52*, 2163 – 2165.

[8] C. Baerlocher, L. B. McCusker, D. H. Olson, *Atlas of Zeolite Framework Types*, 6th rev. ed., Elsevier, Amsterdam, **2007**.

[9] a) O. Sel, D. Kuang, M. Thommes, B. Smarsly, *Langmuir* **2006**, *22*, 2311 – 2322.

[10] a) A. Vantomme, Z. Yuan, B. Su, *New J. Chem.* **2004**, *28*, 1083 – 1085; b) F.-S. Xiao, L. Wang, C. Yin, K. Lin, Y. Di, J. Li, R. Xu, D. Su, R. Schlögl, T. Yokoi, T. Tatsumi, *Angew. Chem.* **2006**, *118*, 3162 – 3165; *Angew. Chem. Int. Ed.* **2006**, *45*, 3090 – 3093; c) X. Meng, F. Nawaz, F.-S. Xiao, *Nano Today* **2009**, *4*, 292 – 301; d) K. Na, C. Jo, J. Kim, K. Cho, J. Jung, Y. Seo, R. J. Messinger, B. F. Chmelka, R. Ryoo, *Science* **2011**, *333*, 328 – 332; e) F. Liu, T. Willhammar, L. Wang, L. Zhu, Q. Sun, X. Meng, W. Carrillo-Cabrera, X. Zou, F.-S. Xiao, *J. Am. Chem. Soc.* **2012**, *134*, 4557 – 4560; f) X. Zhang, D. Liu, D. Xu, S. Asahina, K. A. Cychosz, K. V. Agrawal, Y. Al Wahedi, A. Bhan, S. Al Hashimi, O. Terasaki, M. Thommes, M. Tsapatsis, *Science* **2012**, *336*, 1684 – 1687.

[11] a) T. Komatsu, H. Ikenaga, *J. Catal.* **2006**, *241*, 426 – 434; b) T. Blasco, A. Chica, A. Corma, W. J. Murphy, J. Agúndez-Rodríguez, J. Pérez-Pariente, *J. Catal.* **2006**, *242*, 153 – 161; c) C. Song, Y. Feng, L. Ma, *Microporous Mesoporous Mater.* **2012**, *147*, 205 – 211.

[12] C. Wang, Y. Wang, H. Liu, Z. Xie, Z. Liu, *J. Catal.* **2010**, *271*, 386 – 391.

[13] a) A. M. Prakash, S. Unnikrishnan, *J. Chem. Soc. Faraday Trans.* **1994**, *90*, 2291 – 2296; b) A. Buchholz, W. Wang, M. Xu, A. Arnold, M. Hunger, *Microporous Mesoporous Mater.* **2002**, *56*, 267 – 278; c) G. Liu, P. Tian, Y. Zhang, J. Li, L. Xu, S. Meng, Z. Liu, *Microporous Mesoporous Mater.* **2008**, *114*, 416 – 423.

[14] a) C. S. Blackwell, R. L. Patton, *J. Phys. Chem.* **1984**, *88*, 6135 – 6139; b) C. S. Blackwell, R. L. Patton, *J. Phys. Chem.* **1988**, *92*, 3965 – 3970.

[15] a) D. Hasha, L. S. de Saldarriaga, C. Saldarriaga, P. E. Hathaway, D. F. Cox, M. E. Davis, *J. Am. Chem. Soc.* **1988**, *110*, 2127 – 2135; b) Y. Huang, D. Machado, C. W. Kirby, *J. Phys. Chem. B* **2004**, *108*, 1855 – 1865.

[16] a) H.-L. Zubowa, E. Alsdorf, R. Fricke, F. Neissendorfer, J. Richter-Mendau, E. Schreier, D. Zeigan, B. Zibrowius, *J. Chem. Soc. Faraday Trans.* **1990**, *86*, 2307 – 2312; b) Y. Watanabe, A. Koiwai, H. Takeuchi, S. A. Hyodo, S. Noda, *J. Catal.* **1993**, *143*, 430 – 436.

[17] a) R. B. Borade, A. Clearfield, *J. Mol. Catal.* **1994**, *88*, 249 – 265; b) J. Tan, Z. Liu, X. Bao, X. Liu, X. Han, C. He, R. Zhai, *Microporous Mesoporous Mater.* **2002**, *53*, 97 – 108.

